processes

MDPI

Article

# Critical Hydraulic Gradient of Internal Erosion at the Soil–Structure Interface

**Quanyi Xie, Jian Liu *, Bo Han *, Hongtao Li, Yuying Li and Xuanzheng Li**

School of Civil Engineering, Shandong University, 17922, Jingshi Road, Jinan 250061, China; quanyixiesdu@163.com (Q.X.); 17865131577@163.com or lihongtaosdu@163.com (H.L.); liyuyingsdu@163.com (Y.L.); lixuanzheng1992@163.com (X.L.)

* Correspondence: liujianshanda@163.com (J.L.); bo.han@sdu.edu.cn (B.H.); Tel.: +86-136-1641-9012 (J.L.)

Received: 25 June 2018; Accepted: 16 July 2018; Published: 18 July 2018


**Abstract:** Internal erosion at soil–structure interfaces is a dangerous failure pattern in earth-fill water-retaining structures. However, existing studies concentrate on the investigations of internal erosion by assuming homogeneous materials, while ignoring the vulnerable soil–structure-interface internal erosion in realistic cases. Therefore, orthogonal and single-factor tests are carried out with a newly designed apparatus to investigate the critical hydraulic gradient of internal erosion on soil–structure interfaces. The main conclusions can be draw as follows: (1) the impact order of the three factors is: degree of compaction > roughness > clay content; (2) the critical hydraulic gradient increases as the degree of compaction and clay content increases. This effect is found to be more obvious in the higher range of the degree of soil compaction and clay content. However, there exists an optimum interface roughness making the antiseepage strength at the interface reach a maximum; (3) the evolution of the interface internal erosion develops from inside to outside along the interface, and the soil particles at the interface flow as a whole; and (4) the critical hydraulic gradient of interface internal erosion is related to the shear strength at the interface and the severity and porosity of the soil.

**Keywords:** soil–structure interface; internal erosion; critical hydraulic gradient; orthogonal tests

## 1. Introduction

Internal erosion is the transportation of soil particles induced by internal seepage [1,2]. The current studies broadly categorize internal erosion into four groups: (a) concentrated leak erosion; (b) backward erosion; (c) contact erosion; (d) suffusion. Concentrated leak erosion is the process of sweeping particles away from the side of the crack due to the effect of the seepage [3–5]. Backward erosion refers to the process of generating permeating channels from downstream to upstream due to the action of water flow in strong permeable layers [6–8]. Contact erosion occurs in the interface between particles with different diameters, and the small particles erode into the framework of large particles [9]. Suffusion refers to the phenomenon that small particles in the soil are flowed away from the pore between large particles [10,11]. However, internal erosion between soil and structure is not included in the four types of internal erosion discussed above.

Soil–structure interfaces widely exist in hydraulic structures and the associated interface internal erosion failures significantly threaten engineering safety. In particular, seepage channels can be easily developed through the weak interfaces due to the differential mechanical properties between soil and the structure [12]. This can eventually lead to the formation of pipes/conduits, cavities and unstable zones in earth-fill structures [13]. For instance, the Teton dam in US, with a height of 91.5 m, collapsed in June, 1976. After the accident investigation, the main reason of the dam failure was attributed to the internal erosion at the interface between the clay core wall and rock [14,15].

Although the phenomenon of soil–structure-interface internal erosion has been noticed, existing studies have concentrated on the investigations of internal erosion by assuming homogeneous materials, while ignoring the more vulnerable soil–structure-interface internal erosion in realistic cases. [16–19]. The failure mechanism of interface internal erosion can be more complex and dangerous due to the interaction with the internal affiliated structures [20,21]. The associated interface internal erosions have been frequently observed, such as at the interfaces between cut-off walls and earth-fill materials in dams [22–26], between cut-off walls and earth-fill materials in levees [27–29], and between retaining walls and backfill materials [30–32]. In these works, some empirical criteria are proposed and developed for evaluating the internal stability potential at the soil–structure interface. However, there are few studies on the effects and mechanism of internal erosion at the soil–structure interface.

Therefore, in this paper, a newly designed seepage apparatus is employed to investigate the failure mechanism of internal erosion at soil–structure interfaces. Both orthogonal tests and single-factor tests are designed to investigate the sensitivity of the critical hydraulic gradient of internal erosion subjected to three critical soil properties, that is, degree of compaction, clay content and roughness. The failure mechanism of interface internal erosion is studied by analyzing the observed failure phenomena and the variation of seepage behavior. Furthermore, the relationship between interface shear strength and critical hydraulic gradient is obtained by analyzing the forces on the soil–structure interface for the investigated cases.

## 2. Soil–Structure-Interface Internal Erosion Tests

### *2.1. Soil–Structure Interface Seepage Failure Apparatus*

Figure 1 shows the designed soil–structure interface seepage failure apparatus. The dimensions of the apparatus are 600 × 300 × 1000 mm (length × width × height). The dimensions of the sample container are 500 × 300 × 800 mm. The sample container is made of acrylic plates, and it consists of two parts, the upper sample chamber and the lower seepage transition chamber. The soil and concrete blocks are placed in the upper chamber with the concrete blocks at the two sides and a soil specimen in the middle. The porous boards are divided into two parts, that is, an inclined porous board and a horizontal porous board. The slope of the inclined porous board is 1:1 and it can effectively filter any gas bubbles in the filled water. The inlet and outlet are set into the lower and upper parts of the sample container, respectively (as shown in Figure 1). When the tests are conducted, water flows upward. The testing apparatus is equipped with a constant-head water supply system and a data acquisition system (seepage discharge and hydraulic head are recorded).

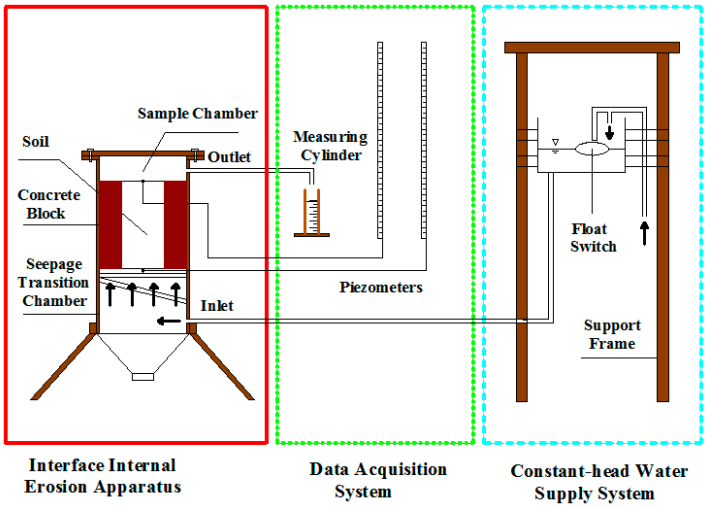


(**a**)

**Figure 1.** *Cont.*

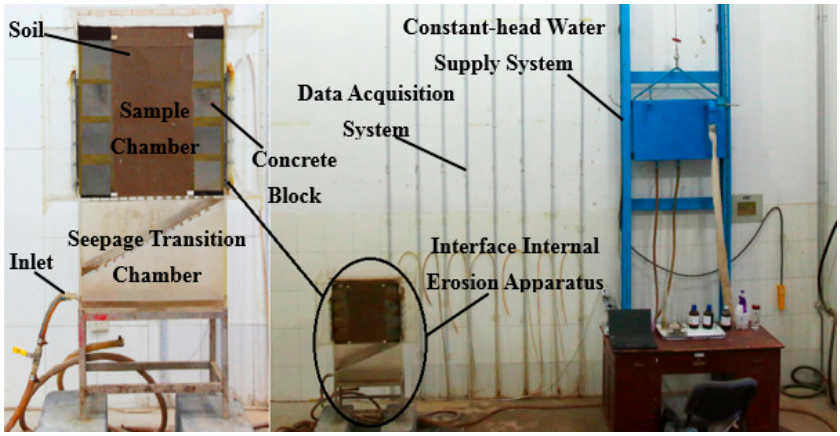


(**b**)

**Figure 1.** Testing apparatus. (**a**) Schematic graph of interface internal erosion testing system; (**b**) physical testing apparatus.

### 2.2. Testing Materials

In reality, when filling soil around concrete buildings, soil of high liquid-plastic limits and high clay particle content is usually used. Therefore, the selection of soil samples in the present work is based on these two factors. The samples for this study are obtained by mixing two soils: silt and clay from the Yellow River alluvial plain. The grain-size distribution curves of the four tested soils are shown in Figure 2. The ranges of clay content and liquid limit of the soil samples are 21.8–29.8% and 31.84–33.78%, respectively, and these cover the concerned soil property ranges for hydraulic engineering structures defined in the Chinese Embankment Dam Constructions Code (DL/T 5395 2007). The material properties and particle compositions of the four tested soils are listed in Table 1.

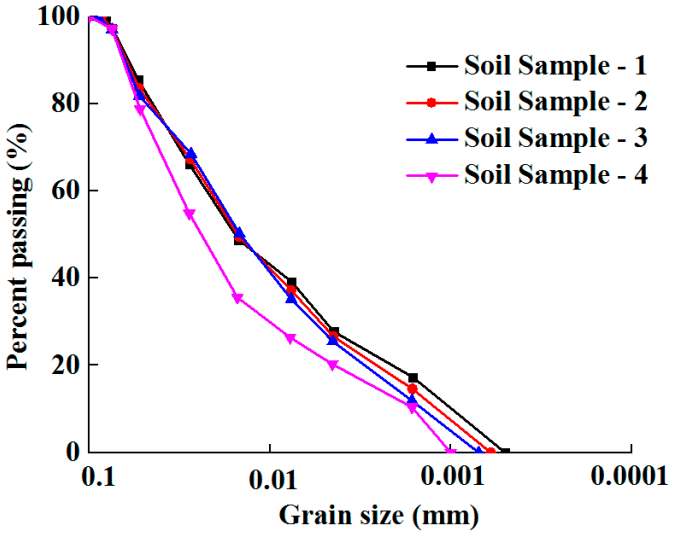


**Figure 2.** Grain-size distribution curves.

**Table 1.** Material properties for the tested soils.

| Material Properties | Soil Sample-1 | Soil Sample-2 | Soil Sample-3 | Soil Sample-4 |
|---|---|---|---|---|
| Clay content (<0.005 mm) (%) | 29.8 | 27.9 | 26.8 | 21.8 |
| Liquid limit (%) | 33.78 | 33.51 | 33.07 | 31.84 |
| Plastic limit (%) | 18.90 | 18.42 | 18.36 | 17.14 |
| Specific gravity | 2.74 | 2.74 | 2.74 | 2.74 |
| Optimal water content (%) | 20.3 | 18.7 | 18.3 | 18.1 |
| Maximum dry density (g/cm$^3$) | 1.660 | 1.672 | 1.678 | 1.683 |

### 2.3. Soil Sample Preparation

Silt and clay are first crushed and mixed in a certain proportion. The mass ratio of silt and clay of samples 1, 2, 3 and 4 are 3:7, 3.5:6.5, 4:6 and 5:5, respectively. In order to ensure full water absorption, optimum water content is maintained when producing the soil samples for 24 h. At the same time, in order to reduce the influence of moisture content in the test, the difference of moisture content between the two sets of soil samples for repeated tests is controlled within 1%.

In order to ensure uniformity of the tested soil samples, the obtained samples are subsequently filled into the upper chamber by controlling a certain degree of compaction. The thickness of each layer is 4 cm. The degree of compaction of soil samples is controlled by controlling the compaction quality of each layer.

The roughness of the soil–structure interface is defined by the height of the salient of the structure. The height of the salient varies by changing the diameter of sand particles that are attached to the structure. For instance, a roughness of 0.3 cm means that the diameter of the sand particles attached to the structure is 0.3 cm.

The hydraulic head in the constant-head water supply system is raised to saturate the soil samples before the tests. The hydraulic head is raised by 1 cm every 1 h. This relatively slow saturation process can reduce the seepage scouring effect on soil samples.

### 2.4. Testing Program

When the tests start, the inlet hydraulic head is gradually raised to the designed values. The piezometric levels of the outflow are recorded, and the outflow seepage discharge is measured every 5 min. When the outflow hydraulic heads and seepage discharge subjected to two sequent hydraulic head raises are sufficiently close, that is, the differences of two results are within 5%, it is considered to reach the steady state. Furthermore, typical failure phenomena, such as water turbidity and slight bulging, are also monitored as the failure criteria during the experiments. When any of the mentioned failure phenomena appear at the soil–structure interface, the tests are continuously observed for 1 to 2 h. Internal erosion is recognized when the hydraulic head cannot be further raised.

### 2.5. Testing Schemes

Orthogonal tests are carried out to analyze the sensitivity of failure mechanisms of interface internal erosion subjected to three critical soil properties (degree of compaction, clay content and roughness). Regardless of the interplay of the factors, the orthogonal table L9 ($3^4$) is used. The designed tables of the influence factor level and the orthogonal tests are listed in Tables 2 and 3, respectively.

On the basis of the orthogonal tests, the single-factor tests are also carried out to investigate in detail the influence of the three factors on interface internal erosion. The designed testing scheme of the single-factor tests is shown in Table 4. In order to ensure the reproducibility and accuracy of the test data, three independent tests are carried out for each test condition. The mean values of the data from the three tests are firstly calculated (that is, the hydraulic gradient-flow velocity curve). If all the data lie in the $\pm$10% deviation range of the mean curve, they are considered to be reliable and the mean curve is used to represent the soil behavior under this specific test condition. Furthermore,

a series of measures are also employed to enhance the reproducibility of the data. In particular, firstly, the deviations of water content and clay content are controlled within 0.5%; secondly, quality control is adopted when reconstituting the sample and the deviation of compactness is controlled within 1%; thirdly, the accuracy of the water supply system is 1 mm and the error is only 2%; last but not least, the accuracy of the seepage discharge measure unit is 0.01 $cm^3$ and the error is 1%.

**Table 2.** Level of influence factors.

| Factor Level | A<br>Degree of Compaction (%) | B<br>Clay Content (%) | C<br>Roughness (cm) |
|---|---|---|---|
| 1 | 80 | 21.8 | 0 |
| 2 | 85 | 26.8 | 0.3 |
| 3 | 90 | 29.8 | 0.6 |

**Table 3.** Testing scheme of orthogonal tests.

| Factor Test Number | A<br>Degree of Compaction (%) | B<br>Clay Content (%) | C<br>Roughness (cm) |
|---|---|---|---|
| I-1 | 80 | 21.8 | 0.6 |
| I-2 | 80 | 26.8 | 0.3 |
| I-3 | 80 | 29.8 | 0 |
| I-4 | 85 | 21.8 | 0.3 |
| I-5 | 85 | 26.8 | 0 |
| I-6 | 85 | 29.8 | 0.6 |
| I-7 | 90 | 21.8 | 0 |
| I-8 | 90 | 26.8 | 0.6 |
| I-9 | 90 | 29.8 | 0.3 |

**Table 4.** Testing scheme of single-factor tests.

| Test Number | Degree of Compaction (%) | Clay Content (%) | Roughness (cm) |
|---|---|---|---|
| II-1 | 90 | 29.8 | 0 |
| II-2 | 87 | 29.8 | 0 |
| II-3 | 85 | 29.8 | 0 |
| II-4 | 80 | 29.8 | 0 |
| II-5 | 85 | 27.9 | 0 |
| II-6 | 85 | 26.8 | 0 |
| II-7 | 85 | 21.8 | 0 |
| II-8 | 85 | 29.8 | 0.6 |
| II-9 | 85 | 29.8 | 0.4 |
| II-10 | 85 | 29.8 | 0.3 |

## 3. Testing Results

### *3.1. Observed Test Phenomena*

The observed phenomena of the soil–structure-interface internal erosion are shown in Figure 3 (soil sample on left, concrete block on right). The presented results show a three-stage failure evolution of interface internal erosion, that is, the stable, transition and failure stages. At the stable and transition stages, no particles flow from the surface of the soil–concrete interface, but the soil at the interface shows a slight bulging (uplift of soil) in the transition stage. At the failure stage, a large number of fine particles are transported along the interface. After the interface internal erosion, a crack is formed at the soil–structure interface (see Figure 3d).

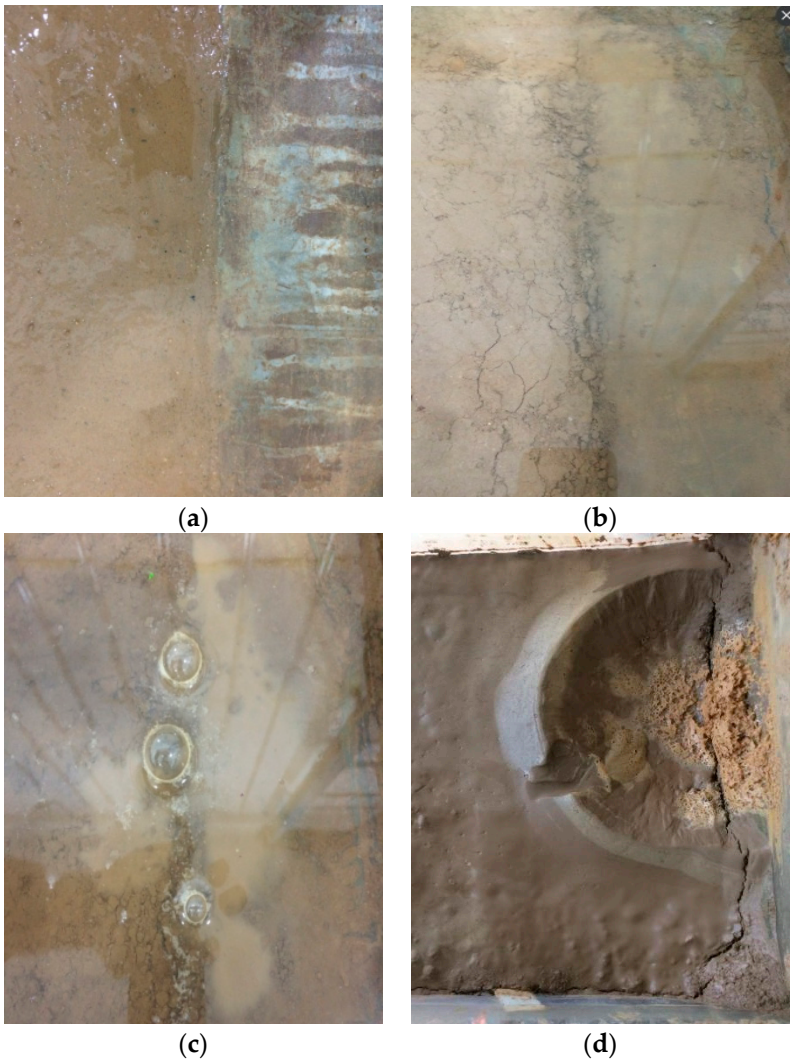


**Figure 3.** Phenomena of soil–structure-interface internal erosion. (**a**) Stable stage; (**b**) transition stage; (**c**) failure stage; (**d**) interface internal erosion.

### *3.2. Mechanism of Interface Internal Erosion*

The relationships of the seepage velocity, hydraulic gradient, permeability coefficient, and the eroded soil mass against time of II-1 (degree of compaction = 90%, clay content = 29.8%, interface roughness = 0) are shown in Figures 4 and 5. In the experiment, the hydraulic gradient is applied by a certain increment. With the increase of hydraulic gradient, it can be seen that the seepage velocity starts to increase, but the average hydraulic coefficient does not change, and no soil particles are flowing from the interface. When the hydraulic gradient increases to 1.63, the average hydraulic coefficient starts to increase, but the soil particles have not been eroded from the interface. This indicates that the soil particles at the interface start to move due to seepage but have not been totally eroded from the interface. When the hydraulic gradient increases to 1.99, a large number of soil particles are rushed out from the interface. At this stage, the interface has been penetrated and destroyed. From Figure 3d, it can be seen that the interface internal erosion is observed as the overall flow of soil particles at the interface. In particular, the infiltration at the interface is developed from the inside to the outside, and a crack is formed at the soil–structure interface.

The critical hydraulic gradient is used to characterize the seepage stability of soil samples, related to soil porosity and density. Critical hydraulic gradient is defined by the hydraulic gradient where particles start to outflow from soil samples. The determination of the critical hydraulic gradient of internal erosion is based on the occurrence of "sand boil" or other indicating phenomena of seepage failure. Therefore, the threshold hydraulic gradient, when soil particles outflow from the interface, is defined as the critical hydraulic gradient for interface internal erosion.

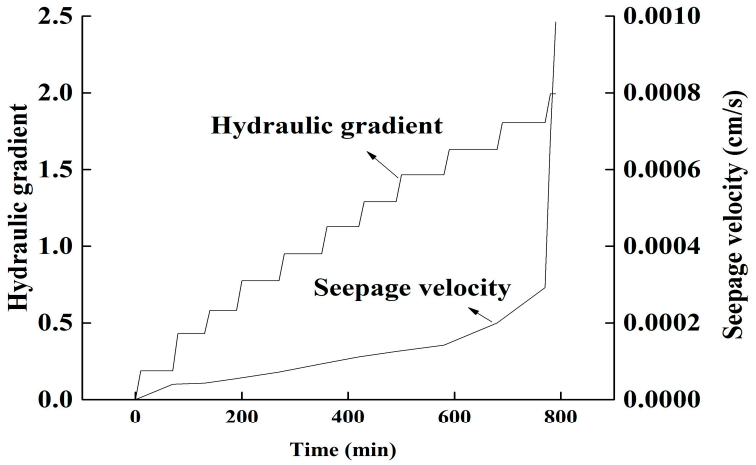


**Figure 4.** Hydraulic gradient and seepage velocity-t curve of II-1.

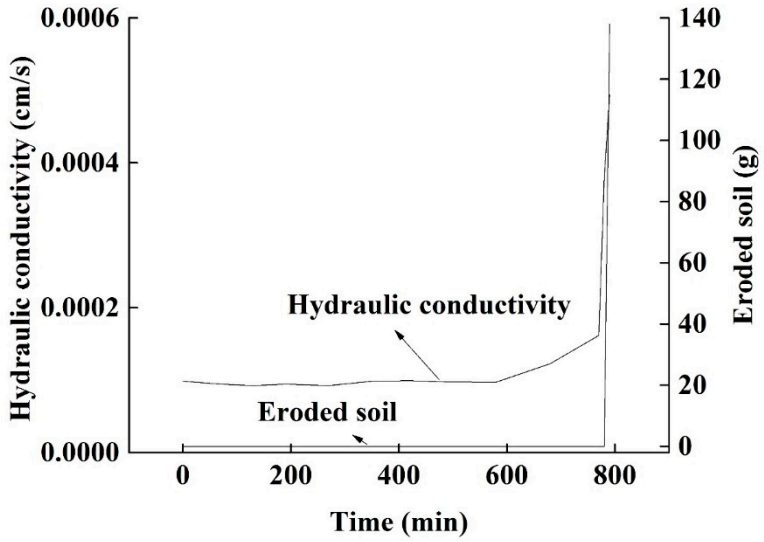


**Figure 5.** Hydraulic conductivity and eroded soil-t curve of II-1.

### *3.3. Orthogonal Test Results*

The results from the orthogonal tests are analyzed and discussed in this section. It is noted that the error analysis, range analysis and variance analysis are carried out to analyze the effect of error and three critical soil property factors.

### 3.3.1. Error Analysis

The critical hydraulic gradients from orthogonal test results are listed in Table 5. SSj is the sum of squares of each factor and SSE is the error sum of squares. In the orthogonal tests, the average critical hydraulic gradient is 1.48. The sum square of degree of compaction is 1.83. The sum square of clay content is 0.23. The sum square of roughness is 0.45. The error sum square of the orthogonal test is 0.04. The error sum square of the orthogonal experiment is much smaller than the sum of squares of the factors. Therefore, the degree of the influence of error in the orthogonal experiment can be neglected.

**Table 5.** Critical hydraulic gradient of orthogonal test results.

| | A<br>Degree of Compaction (%) | B<br>Clay Content (%) | C<br>Roughness (cm) | E<br>Empty Column | Critical Hydraulic Gradient |
|---|---|---|---|---|---|
| I-1 | 1(80) | 1(21.8) | 3(0.6) | 1 | 0.98 |
| I-2 | 1(80) | 2(26.8) | 2(0.3) | 2 | 1.24 |
| I-3 | 1(80) | 3(29.8) | 1(0) | 3 | 1.06 |
| I-4 | 2(85) | 1(21.8) | 2(0.3) | 3 | 1.40 |
| I-5 | 2(85) | 2(26.8) | 1(0) | 1 | 1.00 |
| I-6 | 2(85) | 3(29.8) | 3(0.6) | 2 | 1.31 |
| I-7 | 3(90) | 1(21.8) | 1(0) | 2 | 1.81 |
| I-8 | 3(90) | 2(26.8) | 3(0.6) | 3 | 1.79 |
| I-9 | 3(90) | 3(29.8) | 2(0.3) | 1 | 2.74 |
| SSj | 1.83 | 0.23 | 0.45 | 0.04 | |

### 3.3.2. Range Analysis

The range analysis results are shown in Table 6. $K_1$, $K_2$ and $K_3$ are the average values of critical hydraulic gradient under the same test condition of different factors. The results from the range analysis show that $R_A = 1.02 > R_C = 0.50 > R_B = 0.36$, where RA, RB and RC are the ranges of degree of compaction, clay content and roughness, respectively. This demonstrates that the investigated interface internal erosion is most significantly affected by degree of compaction. The influence of the roughness is relatively less profound, while the clay content shows the least impact.

**Table 6.** Range analysis results of interface internal erosion.

| | A<br>Degree of Compaction (%) | B<br>Clay Content (%) | C<br>Roughness (cm) |
|---|---|---|---|
| $K_1$ | 1.09 | 1.40 | 1.36 |
| $K_2$ | 1.24 | 1.34 | 1.79 |
| $K_3$ | 2.11 | 1.70 | 1.29 |
| Range $R_i$ | 1.02 | 0.36 | 0.5 |

### 3.3.3. Variance Analysis

The data of the variance analysis of orthogonal test results is shown in Table 7. The variance analysis results of orthogonal tests show that the F of degree of compaction is 42, which is greater than $F_{0.025}(2,2)$, and its effect on the critical hydraulic gradient is significant. The F of clay content is 6, which is greater than $F_{0.25}(2,2)$, and its effect on the critical hydraulic gradient is relevant. The F of roughness is greater than $F_{0.10}(2,2)$, and its effect on the critical hydraulic gradient is significant. This is also in agreement with the results from the variance analysis. In particular, the results from the variance analysis show that the significance level of degree of compaction is the highest, followed by roughness and clay content. Therefore, the impact order of the three factors is: degree of compaction > roughness > clay content.

**Table 7.** Variance analysis results of interface internal erosion.

| | A<br>Degree of Compaction (%) | B<br>Fine Content (%) | C<br>Roughness (cm) | E<br>Empty Column |
|---|---|---|---|---|
| $K_{1j}^2$ | 3.28 | 4.19 | 4.08 | 4.72 |
| $K_{2j}^2$ | 3.71 | 4.03 | 5.38 | 4.36 |
| $K_{3j}^2$ | 6.34 | 5.11 | 3.87 | 4.25 |
| Free degree | 2 | 2 | 2 | 2 |
| SS | 1.83 | 0.23 | 0.45 | 0.04 |
| MS | 0.92 | 0.12 | 0.23 | 0.02 |
| F | 42 | 6 | 11.50 | |
| $F_{0.01}(2,2)$ | 99 | 99 | 99 | |
| $F_{0.025}(2,2)$ | 39 | 39 | 39 | |
| $F_{0.05}(2,2)$ | 19 | 19 | 19 | |
| $F_{0.10}(2,2)$ | 9 | 9 | 9 | |
| $F_{0.25}(2,2)$ | 3 | 3 | 3 | |
| Significance level | ** (Greatly significant) | - (Relevant) | * (Significant) | |

### 3.4. Effect of Degree of Compaction

Figure 6 shows the hydraulic gradient–seepage velocity curves under different degrees of compaction. The degrees of compaction of the tests II-1, II-2, II-3 and II-4 are 80%, 85%, 88% and 90%, respectively. The relationship between hydraulic gradient and seepage velocity of three degrees of compaction is characterized by three stages. Figure 7 plots the variations of the critical hydraulic gradient against degree of compaction. When the soil degree of compaction increases from 80% to 85%, the hydraulic gradient increases by 10.47%. However, when the degree of compaction increases from 85% to 90%, the hydraulic gradient increases by 70.86%. It indicates the strengthening effects of soil compaction against seepage-induced interface deformation. This effect is found to be more obvious in the higher range of the degree of soil compaction, that is, a higher increase rate.

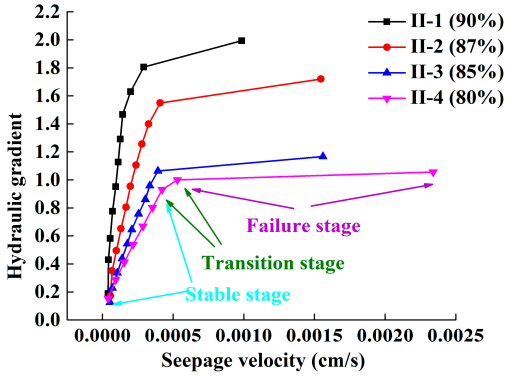


**Figure 6.** Hydraulic gradient–seepage velocity curves under different degrees of compaction.

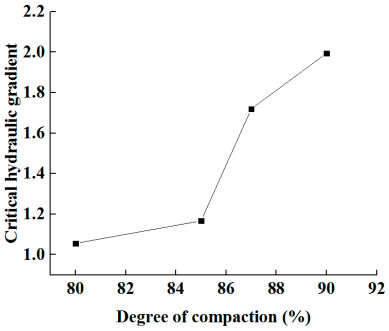


**Figure 7.** Critical hydraulic gradients for different degrees of compaction.

### *3.5. Effect of Interface Roughness*

The hydraulic gradient–seepage velocity behavior under different roughness conditions is shown in Figure 8. The results reflect the impact of interface roughness (bonding between the soil and structure) on interface internal erosion. The interface roughnesses of the tests II-3, II-8, II-9 and II-10 are 0, 0.3, 0.4 and 0.6 mm, respectively. It can be seen that as interface roughness increases, the critical hydraulic gradient first increases, reaches the peak at 0.3 mm roughness and then decreases. This is also reflected by the critical hydraulic gradient–interface roughness relation in Figure 9. The presented results indicate an optimum interface roughness where the highest antiseepage strength can be obtained against interface internal erosion. The reason for the optimum interface roughness is that when the soil–structure interface is relatively smooth, soil particles can be easily transported by seepage water and therefore the critical hydraulic gradient is low. When interface roughness is higher, the antiseepage strength and the critical hydraulic gradient are larger as a consequence of a bigger friction at the interface. However, after reaching a threshold value, the voids between soil and structure are so large that a more significant water flow generates and therefore leads to a lower critical hydraulic gradient, as illustrated in Figure 10. The optimum roughness is found to be approximately 0.3 mm for the investigated cases.

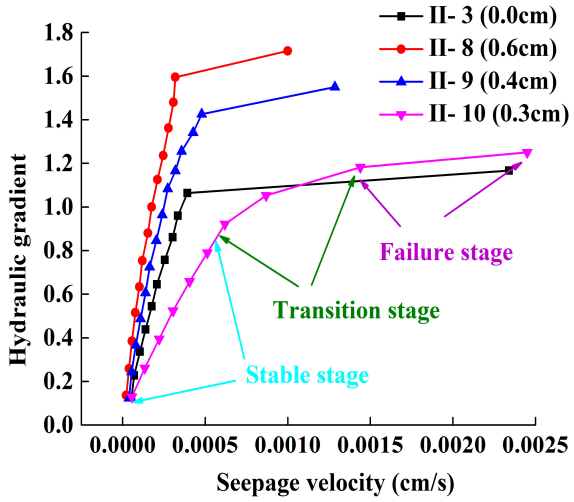


**Figure 8.** Hydraulic gradient–seepage velocity curves under different roughnesses.

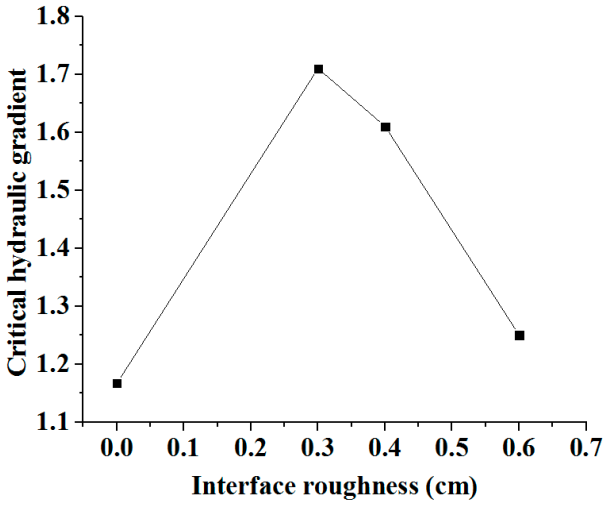


**Figure 9.** Critical hydraulic gradients for different roughnesses.

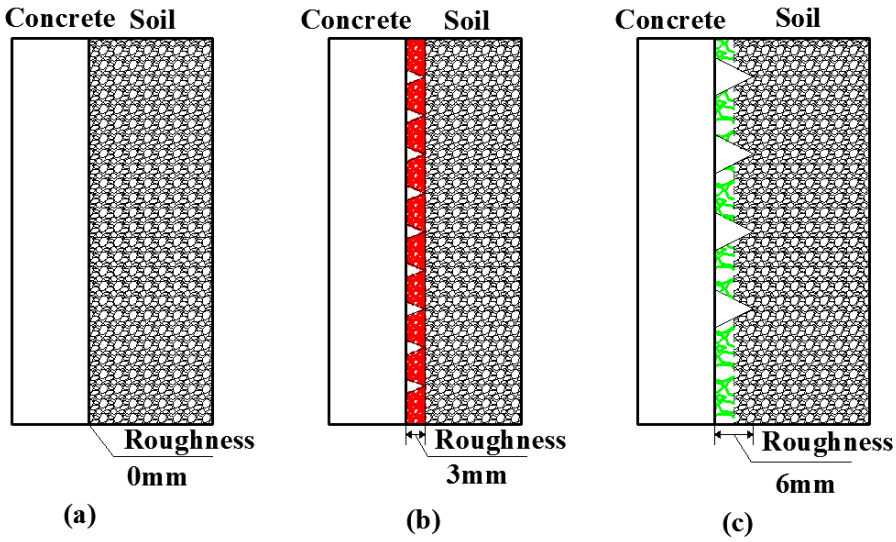


**Figure 10.** Schematic graph for different interface roughnesses. (**a**) Schematic graph for the interface roughness of 0 mm; (**b**) schematic graph for interface roughness of 3 mm; (**c**) schematic graph for interface roughness of 6 mm.

### *3.6. Effect of Clay Content*

The hydraulic gradient–seepage velocity behavior plots under different clay contents are shown in Figure 11. It can be seen that the difference between the results from II-6 and II-7 tests is negligible, indicating the insignificant effect of clay content in its low range. However, by comparing the results from II-3, II-5 and II-6, it shows that in the higher range of clay content, the critical hydraulic gradient increases more significantly as the clay content increases, and the stable seepage stage is also obviously prolonged. Figure 12 further plots the variations of critical hydraulic gradients against clay contents. When the clay content of soil increases from 21.8% to 26.8%, the critical hydraulic gradient increment is negligible. However, when the clay content of soil increases from 26.8% to 29.8%, the critical hydraulic gradient increases by 18%. It is obvious that the critical hydraulic gradient of interface internal erosion presents a piecewise functional relationship with the increase of clay content. When the clay content increases to 26.8%, the increase of clay content of soil can significantly improve the critical hydraulic gradient under the experimental conditions.

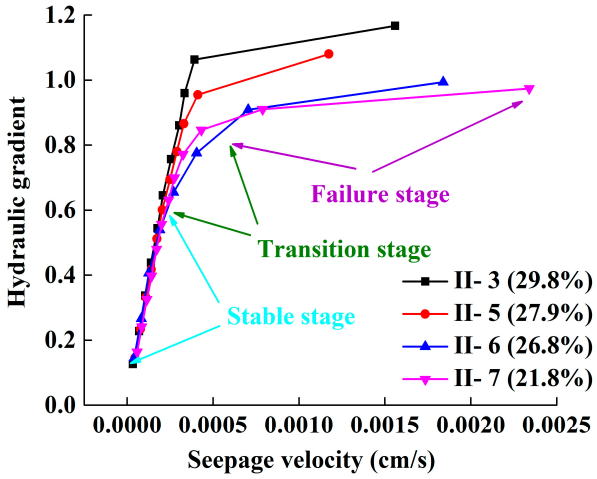


**Figure 11.** Hydraulic gradient–seepage velocity curves under different clay contents.

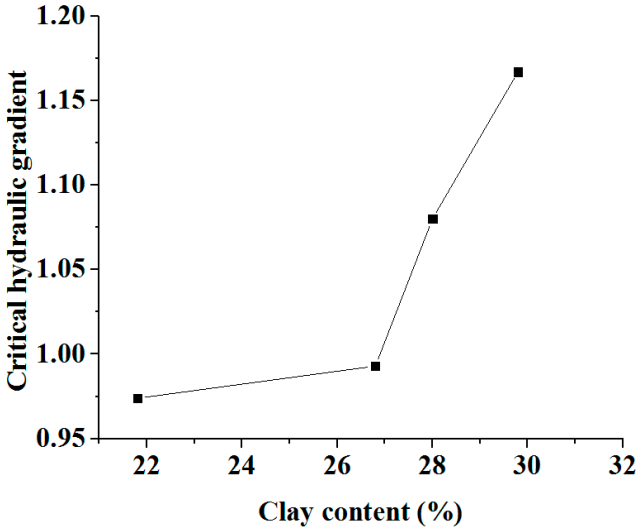


**Figure 12.** Critical hydraulic gradients for different clay contents.

## 4. Discussion of Critical Hydraulic Gradient

The critical hydraulic gradient of internal erosion is mostly calculated by limit balance equilibrium of forces in soil units. In this section, the critical hydraulic gradient of interface internal erosion is studied by analyzing the forces imposed on soil particles. Furthermore, a section of soil and concrete is selected as the control body (height: $dz$, thickness: $da$). The soil–structure shear strength is expressed by the maximum shear stress. The forces acting on soil particles in the control body are shown in Figure 13. They are discussed as follows:

The volume force acting on the soil particles can be expressed as:

$$f_z = r_\omega \frac{dh}{dz}. \tag{1}$$

The shear force between soil and concrete in the control body is defined as:

$$2\tau dadz. \tag{2}$$

The submerged unit weight of the soil particles at the interface is expressed as:

$$\gamma' = \gamma_\omega (Gs - 1)(1 - n). \tag{3}$$

When interface internal erosion occurs, the soil particles on the interface are in the limit equilibrium state, where the submerged unit weight of soil particles plus the shear force between soil and concrete is equal to the volume force loaded on the soil particles by water.

After substituting Equations (2) and (3) into Equation (1), the critical hydraulic gradient of interface internal erosion can be written as Equation (4):

$$i_{cr} = \frac{dh}{dz} = (Gs - 1)(1 - n) - \frac{2\tau da}{A\gamma_\omega} \tag{4}$$

The definition of symbols in the Equation (4) are shown in Table 8. According to Equation (4), critical hydraulic gradient is related to the shear strength of the interface and the severity and porosity of soil. The degree of compaction and clay content of soil affect the impermeability of soil–structure-interface internal erosion through changing the porosity and severity of soil. The interface roughness mainly affects the shear strength of the soil–structure interface. In order

to improve the critical hydraulic gradient of soil–structure internal erosion, measures aiming to enhance the soil–structure shear stress or the impermeability of soil should be adopted.

**Table 8.** Definition of symbols.

| Symbol | Definition |
|---|---|
| *dh* | the hydraulic head differentials between the two ends of the control body |
| *dp* | the water pressure differentials between the two ends of the control body |
| *n* | the porosity of soil |
| *A* | cross-sectional area of soil |
| *dz* | the height of control body |
| $\gamma_\omega$ | unit weight of water |
| $f_z$ | the volume force acting on the soil particles' unit volume |
| $\tau$ | the shear stress between soil and concrete |
| *da* | the thickness of control body |
| *Gs* | specific gravity of soil particles |

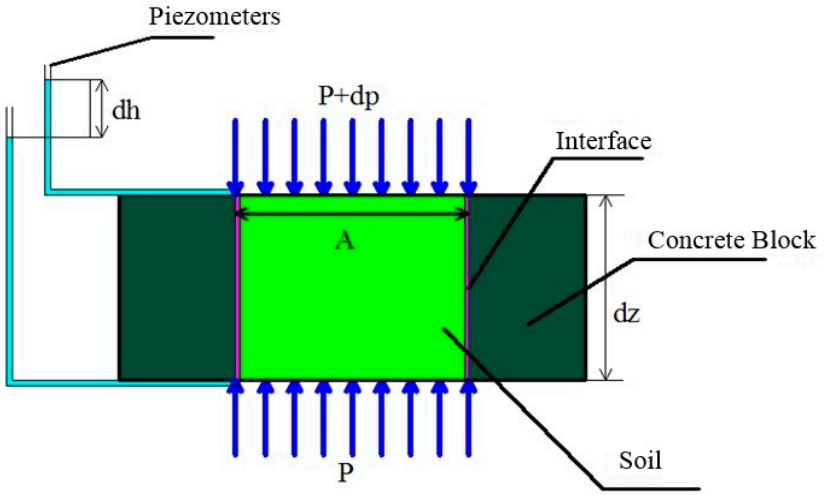


**Figure 13.** Forces acting on soil particles in the control body.

## 5. Conclusions

This paper employed a newly designed seepage apparatus to investigate the failure mechanism of internal erosion at the soil–structure interface. Orthogonal and single-factor tests were designed to investigate the sensitivity of the critical hydraulic gradient of internal erosion subjected to three critical soil properties, that is, degree of compaction, clay content and roughness. Furthermore, the limit equilibrium state method was used to analyze the critical hydraulic gradient of interface internal erosion. Based on the experimental results, the following conclusions can be drawn:

(1) The impact order of the three factors on the critical hydraulic gradient of interface internal erosion is: degree of compaction > roughness > clay content.
(2) The critical hydraulic gradient increases as the levels of degree of compaction and clay content increase. This effect is found to be more obvious in the higher range of the degree of soil compaction and clay content. However, there exists an optimum interface roughness where the highest anti seepage strength can be obtained against interface internal erosion. This optimum roughness is found to be approximately 0.3 mm for the investigated cases.
(3) The evolution of the interface internal erosion develops from inside to outside along the interface, and the soil particles on the interface flow as a whole.

(4) The critical hydraulic gradient of interface internal erosion is related to the shear strength of the interface and the severity and porosity of the soil. The degree of compaction and clay content of soil affect the impermeability of the soil–structure-interface internal erosion through changing the porosity and severity of soil. The interface roughness mainly affects the shear strength of the soil–structure interface.

**Author Contributions:** Q.X., J.L. and B.H. conceived of and designed the study. Q.X., Y.L., X.L. and H.L. performed the experiments. Q.X., J.L., B.H., Y.L., X.L. and H.L. wrote and modified the paper.

**Funding:** This research was funded by the National Science and Technology Support Program of China, grand number is 2015BAB07B05; National Natural Science Foundation of China, grand number is 41172267; and National Natural Science Foundation of China, grand number is 51508310.

**Conflicts of Interest:** The authors declare no conflicts of interest.

## References

1. Sato, M.; Kuwano, R. Suffusion and clogging by one-dimensional seepage tests on cohesive soil. *Soils Found.* **2015**, *55*, 1427–1440. [CrossRef]
2. Horikoshi, K.; Takahashi, A. Suffusion-induced change in spatial distribution of fine fractions in embankment subjected to seepage flow. *Soils Found.* **2015**, *55*, 1293–1304. [CrossRef]
3. Poesen, J.; Luna, E.D.; Franca, A.; Nachtergaele, J.; Govers, G. Concentrated flow erosion rates as affected by rock fragment cover and initial soil moisture content. *Catena* **1999**, *36*, 315–329. [CrossRef]
4. Marot, D.; Bendahmane, F.; Rosquoet, F.; Alexis, A. Internal flow effects on isotropic confined sand-clay mixtures. *J. Soil Contam.* **2009**, *18*, 294–306. [CrossRef]
5. Mercier, F.; Bonelli, S.; Golay, F.; Anselmet, F.; Philippe, P.; Borghi, R. Numerical modelling of concentrated leak erosion during hole erosion tests. *Acta Geotech.* **2015**, *10*, 1–14. [CrossRef]
6. Beek, V.M.V.; Sellmeijer, J.B.; Barends, F.B.J.; Bezuijen, A. Initiation of backward erosion piping in uniform sands. *Géotechnique* **2014**, *64*, 927–941. [CrossRef]
7. Bendahmane, F.; Marot, D.; Alexis, A. Experimental parametric study of suffusion and backward erosion. *J. Geotech. Geoenviron. Eng.* **2008**, *134*, 57–67. [CrossRef]
8. Richards, K.S.; Reddy, K.R. Experimental investigation of initiation of backward erosion piping in soils. *Géotechnique* **2012**, *62*, 933–942. [CrossRef]
9. Germer, L.H. Physical processes in contact erosion. *J. Appl. Phys.* **1958**, *29*, 1067–1082. [CrossRef]
10. Ke, L.; Takahashi, A. Experimental investigations on suffusion characteristics and its mechanical consequences on saturated cohesionless soil. *Soils Found.* **2014**, *54*, 713–730. [CrossRef]
11. Yacine, S.; Didier, M.; Luc, S.; Alain, A. Suffusion tests on cohesionless granular matter. *Eur. J. Environ. Civ. Eng.* **2011**, *15*, 799–817. [CrossRef]
12. Luo, Y.L.; Zhan, M.L.; Sheng, J.C.; Qiang, W. Hydro-mechanical coupling mechanism on joint of clay core-wall and concrete cut-off wall. *J. Cent. South. Univ.* **2013**, *20*, 2578–2585. [CrossRef]
13. Kaoser, S.; Barrington, S.; Elektorowicz, M.; Ayadat, T. The influence of hydraulic gradient and rate of erosion on hydraulic conductivity of sand-bentonite mixtures. *Soil Sediment Contam. An Int. J.* **2006**, *15*, 481–496. [CrossRef]
14. Armando, B.; Scheffler, M.L. Numerical analysis of the teton dam failure flood. *J. Hydraul. Res.* **1982**, *20*, 317–328. [CrossRef]
15. Muhunthan, B.; Pillai, S. Teton dam, USA: Uncovering the crucial aspect of its failure. *Civ. Eng.* **2008**, *161*, 35–40. [CrossRef]
16. Boulon, M.; Nova, R. Modelling of soil–structure interface behaviour a comparison between elastoplastic and rate type laws. *Comput. Geotech.* **1990**, *9*, 21–46. [CrossRef]
17. Shahrour, I.; Rezaie, F. An elastoplastic constitutive relation for the soil–structure interface under cyclic loading. *Comput. Geotech.* **1997**, *21*, 21–39. [CrossRef]
18. Hu, L.; Pu, J. Testing and modeling of soil–structure interface. *J. Geotech. Geoenviron. Eng.* **2004**, *130*, 851–860. [CrossRef]
19. Zhang, G.; Zhang, J.M. Large-scale apparatus for monotonic and cyclic soil–structure interface test. *ASTM Geotech. Test. J.* **2006**, *29*, 401–408. [CrossRef]

20. Ferdos, F.; Wörman, A.; Ekström, I. Hydraulic conductivity of coarse rockfill used in hydraulic structures. *Transp. Porous Media* **2015**, *108*, 1–25. [CrossRef]
21. Kim, H.; Park, J.; Shin, J. Flow behaviour and piping potential at the soil–structure interface. *Géotechnique* **2018**, 1–6. [CrossRef]
22. Luo, Y.L.; Wu, Q.; Zhan, M.L.; Sheng, J.C. Study of critical piping hydraulic gradient of suspended cut-off wall and sand gravel foundation under different stress states. *Rock Soil Mech.* **2012**, *36*, 73–78. [CrossRef]
23. Maeda, K.; Sakai, H.; Sakai, M. Development of seepage failure analysis method of ground with smoothed particle hydrodynamics. *Struct. Eng.* **2006**, *23*, 307–319. [CrossRef]
24. Maeda, K.; Sakai, H. Seepage failure and erosion of ground with air bubble dynamics. *Geotech. Spec. Publ.* **2010**, *204*, 261–266. [CrossRef]
25. Liu, R.; Li, B.; Jiang, Y. Critical hydraulic gradient for nonlinear flow through rock fracture networks: The roles of aperture, surface roughness, and number of intersections. *Adv. Water Resour.* **2016**, *88*, 53–65. [CrossRef]
26. Liu, R.; Jiang, Y.; Li, B.; Wang, X. A fractal model for characterizing fluid flow in fractured rock masses based on randomly distributed rock fracture networks. *Comput. Geotech.* **2015**, *65*, 45–55. [CrossRef]
27. Ervin, M.C.; Benson, N.D.; Morgan, J.R.; Pavlovic, N. Melbourne's southbank interchange: A permanent excavation in compressible clay. *Can. Geotech. J.* **2004**, *41*, 861–876. [CrossRef]
28. Wang, B.T.; Chen, X.A. Research on effect of suspended cut-off wall with simulation test. *Chin. J. Rock Mech. Eng.* **2008**, *27*, 2766–2771.
29. Shao, S.J.; Yang, C.M. Research on the impermeability design method of the slurry protection diaphragm wall in the coarse-grained soil foundation. *J. Hydraul. Eng.* **2015**, *46*, 46–53.
30. Barrospérsio, L.A.; Santospetrucio, J. Coefficients of active earth pressure with seepage effect. *Can. Geotech. J.* **2012**, *49*, 651–658. [CrossRef]
31. Wang, S.; Chen, J.S.; Luo, Y.L.; Sheng, J.C. Experiments on internal erosion in sandy gravel foundations containing a suspended cut-off wall under complex stress states. *Nat. Hazards* **2014**, *74*, 1163–1178. [CrossRef]
32. Wang, J.; Zhang, H.; Liu, M.; Chen, Y. Seismic passive earth pressure with seepage for cohesionless soil. *Mar. Georesour. Geotechnol.* **2012**, *30*, 86–101. [CrossRef]